Analysis of MTDC Inertia Emulation Impact on Connected AC Systems

Shuyao Wang
CURENT, Department of EECS
The University of Tennessee
Knoxville, TN, USA
swang67@vols.utk.edu

Shuoting Zhang
CURENT, Department of EECS
The University of Tennessee
Knoxville, TN, USA
zshuotin@vols.utk.edu

Yiwei Ma
CURENT, Department of EECS
The University of Tennessee
Knoxville, TN, USA
yma13@utk.edu

Fred Wang
CURENT, Department of EECS
The University of Tennessee
Oak Ridge National Lab
Knoxville, TN, USA
fred.wang@utk.edu

Leon M. Tolbert
CURENT, Department of EECS
The University of Tennessee
Oak Ridge National Lab
Knoxville, TN, USA
tolbert@utk.edu

***Abstract*— The frequency decoupling effect of the voltage source converter (VSC)-based high voltage dc (HVDC) transmission makes frequency support unavailable between two ac subsystems interconnected by the HVDC link. Recently, several algorithms have been proposed and demonstrated to improve the ac system stability by implementing inertia emulation (IE) functions in the HVDC VSC stations. However, the capability of the VSC-HVDC to achieve the IE control is not clear. According to the previous research, the IE control strategy has been studied without concerning the impact of the practical control process, which will introduce some time delay into the IE realization. In this paper, a detailed multi-terminal HVDC VSC control module, including the phase-locked loop (PLL) and low pass filter (LPF), is considered in order to analyze the multi-terminal HVDC network impact on the IE performance. The analysis indicates that the frequency performance of the ac network with IE integrated HVDC transmission can be nearly as good as that directly connected with the ac subsystem which involves a high penetration of conventional generation units, except for the short time delay introduced by the VSC control modules. The effectiveness of IE performance will be compromised if the response delay is significant. The simulation results have verified the analysis.**

Keywords—multi terminal HVDC, inertia emulation, phase-locked loop, VSC

I. INTRODUCTION

The voltage source converter based high-voltage dc (VSC-HVDC) transmission system is accepted as the solution for long distance bulk power transmission because of its attractive features, including the flexible reactive power support, small size of filters, ability to work with weak grid, small power loss, and black-start capability [1-3].

The HVDC transmission system is widely used in connecting the renewable power sources, which are usually located remotely. One of the most important application of the HVDC transmission is to provide connection between the remote wind farm and the local ac network. The most elementary HVDC wind power transmission system consists of a wind farm connected to a rectifier, a dc power transmission line, and an inverter connecting the dc system to the local ac grid [4]. The point-to-point connection of the remote wind farm with the existing ac grids presents important drawbacks related to the reliability and flexibility of operation, which will limit the wind power capacity. Alternatively, a multi-terminal HVDC (MTDC) network is regarded as a flexible solution for future large-scale remote wind power integration. For either aforementioned two network configurations, the dc link decouples the frequencies from the wind farm end and ac grid end. Thus, a variation in the local ac grid frequency is not reflected on the wind farm side [5-7]. So the remote wind farms cannot rely on the frequency locally measured to contribute to inertia as well as participate in primary frequency control in the way that the local wind farms are able to do. Therefore, the large-scale integration of wind energy will lead to a significant decrease of system inertia as a result of the displacement of conventional generation units. As explained in [8], the inertial frequency response is usually provided instantaneously after a system disturbance and will last for up to a few seconds. Generally, the inertia will act to mitigate any frequency deviation by using the kinetic energy stored in the rotating mass of synchronous generators (SG) and motors. When the system exhibits lower inertia, relatively larger system frequency deviations will result from similar levels of power imbalance, leading to various system stability issues such as faster and more extreme system dynamics, higher rates of change of frequency (RoCoF), and potential problems associated with loss of synchronism [8-9].

Some literatures have covered how to improve power system stability with high renewable energy sources penetration and low system inertia. For example, in [10-13], energy storage (ES) systems were used to provide inertial response; in [14-15] the demand side management was utilized to solve the issue. Another frequently used method for the high wind power penetration network is the HVDC inertia emulation (IE), which will emulate a specific inertia constant by adjusting the control

method of either local converters or remote converters. Several algorithms have been proposed and demonstrated to improve the ac system stability by implementing IE functions in the HVDC VSC stations.

In [3], [16-17] an inertia emulation control strategy was proposed which utilized the energy stored in the dc link capacitors of the HVDC or MTDC systems to emulate the inertial support. The energy stored in the dc link capacitors is transferred to the ac system by adjusting the reference dc link voltage proportionally to the deviation of the ac system frequency after a disturbance.

In [4], [18-19] a communication-free control scheme applying to both the onshore and offshore converters was proposed. By applying appropriate *v-f* droop characteristics on both the onshore and offshore converters, the frequency variation on the onshore side will be transferred to the offshore side so that the wind farm rotating mass will response to such frequency deviation.

In [5],[20] a control method was proposed for HVDC/ MTDC systems which utilized both the energy stored in the dc link and the wind farm active power capacity by appropriately applying control algorithms to both the local converters and the wind farm side converters.

However, little research related to the capability of the VSC-HVDC to achieve the IE control has been addressed. The synchronous generator inertial frequency response will instantaneously regulate the system frequency when there is a grid power mismatch, i.e. the inertial response which results from the generation and demand imbalance will mitigate the grid frequency deviation. However, the system frequency deviation is generally used as the indicator of power imbalance in the IE control design, which is in reverse order compared with that of the SG inertial response. Therefore, the HVDC inertia emulation algorithm is not only required to inject a certain amount of active power, but also required to function as fast as possible regarding a system power mismatch. So the impact of the practical control process on the IE accuracy and efficiency needs to be considered. In this paper, a detailed VSC control module, including the phase-locked loop (PLL) and low pass filter (LPF), is considered in order to analyze the MTDC network impact on the IE performance. The analysis indicates that the frequency performance of the ac network with IE integrated HVDC transmission can be nearly as good as that directly connected with the high inertia ac subsystem, except for the short time delay introduced by the VSC control modules. The effectiveness of IE performance will be compromised if the response delay is significant. The simulation results have verified the analysis.

The structure of the paper is organized as follows: Part II introduces the principle of the inertial response, the MTDC system model and the IE control method that is evaluated in this paper. Part III presents the transfer function of the IE control. Part IV provides the simulation results illustrating the effectiveness of this technique.

II. System Inertia Response and MTDC System Model

In this section, an wind farm integrated ac system with MTDC is introduced since the wind power integration is one of the most important application of the HVDC. However, it should be clarified that the remote side power source is not necessarily to be wind power. Generally, it can be any ac system which is able to provide active power to the local ac network.

A. System Inertial Response Principle

Conventional synchronous generators are widely used in today's electric grid. The kinetic energy expressed in (1), which is noted as E_{kin}, is stored in the rotating mass of the generators or motors.

$$E_{kin} = \frac{1}{2} J\omega^2 \tag{1}$$

where ω is the machine nominal speed of rotation in rad/s, J is the moment of inertia of the rotating mass in kgm^2.When there is a power imbalance between the power supply and demand, the kinetic energy stored in rotating machines will instantaneously be released or consumed during the speed change.

The inertia constant is defined to be the time duration during which the machine can supply its rated power solely by the kinetic energy stored in the rotating mass [21], which is expressed in (2):

$$H = \frac{E_{kin}}{S_{rated}} = \frac{J(2\pi f_m)^2}{2S_{rated}} \tag{2}$$

where S_{rated} is the generator rated power, f_m is the rotating frequency of the machine, and the inertia constant is noted as H in seconds.

The ac system inertial response during a large frequency disturbance is considered as the aggregate effect of all the SGs in the system, which will have a critical influence on the RoCoF in a traditional ac network. Assume the initial rotating frequency is f_0, the relation between the inertia constant H and the kinetic power ΔP is expressed in (3):

$$\frac{2H}{f_0} \cdot \dot{f} = \Delta P \ (p.u.) \tag{3}$$

where f is the frequency of the ac network in Hz.

B. MTDC System Model

The overall structure of a wind farm integrated system using VSC-HVDC transmission is illustrated in Fig. 1. The HVDC system under test in this paper is a four-terminal HVDC network. The constant active, reactive power control, which is referred to as *PQ* control, is applied to the VSC1, VSC2 and VSC4. The constant dc link voltage and constant reactive power control is applied to VSC3, which is referred to as *VQ* control. The *C* represents the converter dc link capacitance. In order to exclusively analyze the impact exerted by the MTDC network, each remote wind farm is simplified as an ideal synchronous generator, which is also illustrated in Fig. 1. So SG1 and SG2 which are located in the previous remote wind farm side are noted as remote SGs in the following paragraph. The simplified

Northeast Power Coordinating Council (NPCC) system model is employed as the main ac grid model [22].

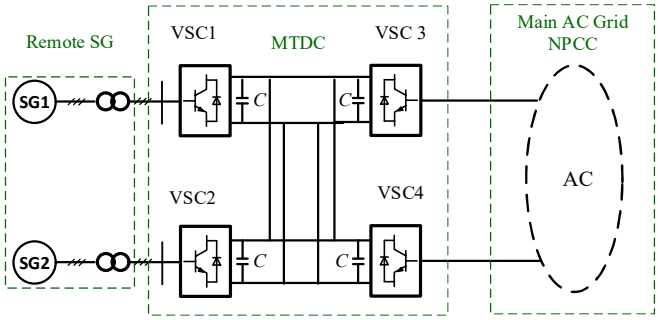

Fig. 1. Simplified wind farm integrated system with multi-terminal HVDC transmission.

C. VSC Inertia Emulation Control

The emulated inertial support is realized by integrating IE control to the HVDC VSC stations. The coordinated IE control strategy is used in this paper, which features using both the electric energy stored in dc link capacitors and the energy transferred from the remote grid side based on the variation of the main ac grid frequency [5, 18-20]. So both the local VSCs and remote VSCs are required to employ IE control. In order to integrate IE control into the *VQ* control of VSC3, the dc link voltage reference $V_{dc,ref}$ changes according to the deviation of the ac grid frequency, which is expressed in (4):

$$K_C \cdot (f_{meas} - f_{nom}) + V_{dc,nom} = V_{dc,ref} \tag{4}$$

where K_C is the proportional control parameter of VSC3, f_{nom} is the initial frequency reference, f_{meas} is the real time grid frequency, $V_{dc,nom}$ is the initial dc link voltage reference. The active power contribution of the dc link capacitors after system disturbance is expressed in (5):

$$\Delta P_{VSC3}(p.u.) = \frac{NCV_{dc,nom}}{S_{VSC}} \cdot \frac{dV_{dc,ref}}{dt} = \frac{NK_CCV_{dc,nom}}{S_{VSC}} \cdot \frac{df_{meas}}{dt} \tag{5}$$

where N is the number of the dc link capacitors, S_{VSC} is the rated power of the VSC3. The dc link capacitors will release or store energy following the change of the ac grid frequency according to (5).

Accordingly, the control diagram for VSC3 is illustrated in Fig. 2(a).

There are usually multiple remote VSC stations in the MTDC system, and all of them can be involved in the IE control. So the remote VSC1 and VSC2 can both employ IE control. The main ac grid frequency performance will be transferred to the remote VSC stations through dc link voltage V_{dc} according to (4) since the voltage deviation is proportional to that of the deviation of the ac grid frequency f_{meas}. The VSC1 or VSC2 will adjust the active power output reference P_{ref} according to the rate of change of the V_{dc}. The active power contribution of one single remote VSC is expressed in (6):

$$\Delta P_W(p.u.) = K_W \frac{dV_{dc}(p.u.)}{dt} = \frac{K_CK_W}{V_{dcref}} \cdot \frac{df}{dt} \tag{6}$$

where K_W is the control parameter of the remote VSC stations. Accordingly, the control diagram of the VSC1 or VSC2 is illustrated in Fig. 2(b). Substitute (5) and (6) into (3), the equivalent inertia constant is expressed in (7):

$$H_S = \frac{NK_CCV_{dc0}f_0}{2S_{VSC}} + \frac{M}{2} \cdot \frac{K_CK_Wf_0}{V_{dcref}} \tag{7}$$

where H_S is the equivalent system inertia constant, M is the number of the remote VSCs that are involved in the IE control. According to Fig. 1, M will be either 1 or 2.

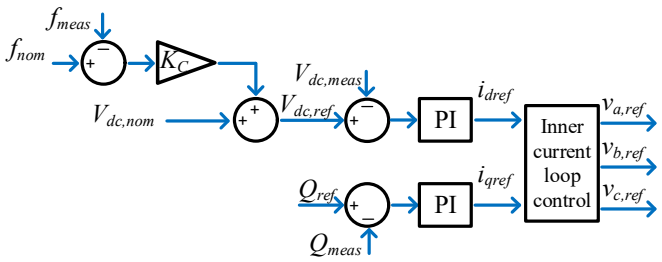

(a) Local VSC3 control method

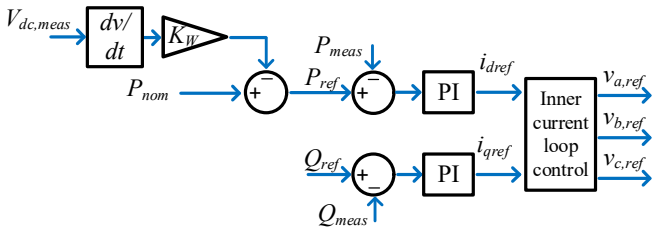

(b) Remote VSC1 control method

Fig. 2. Inertia emulation control strategy for the local and remote HVDC VSC stations.

III. HVDC Impact Analysis

To simplify the analysis, the IE control is implemented in VSC1 at the remote side and VSC3 at the local side. The IE control transfer function can be derived following (4)-(7), of which the input is the ac system frequency per unit value $f_{ac,pu}$ and the output is the active power contribution ΔP_{pu} provided from the local side VSC3.

A. Inertia Emulation Transfer Function

As illustrated in Fig. 2(a), the real time dc link voltage V_{dc} will follow the reference dc voltage $V_{dc,ref}$ if the VSC controller is appropriately designed. Therefore the real time V_{dc} can be expressed as (8).

$$V_{dc} = V_{dc,ref} \cdot \frac{1}{1+s\tau} \tag{8}$$

where τ is the control time constant in seconds.

According to (4) and (5), the $V_{dc,ref}$ is determined by the deviation of the system frequency after the disturbance, and the change of V_{dc} will release/ consume the active power in dc link capacitors, which is expressed as (9):

$$P_{VS}\ \ (p.u.) = \frac{V_{dc,nom} \cdot N \cdot C}{P_{ref}} \cdot \frac{dV_{dc}}{dt} \tag{9}$$

According to (6), the per unit value of the active power reference for VSC1 will change with the rate of change of V_{dc} after a disturbance, which is described as (10) and (11):

$$\Delta P_{ref}(p.u.) = K_W \cdot s \cdot V_{dc} \frac{1}{V_{dc,nom}} \tag{10}$$

$$P_{ref}(p.u.) = P'_{ref}(p.u.) - \Delta P_{ref}(p.u.) \tag{11}$$

where ΔP_{ref} represents the VSC1 reference active power deviation due to the ac system frequency change.

Therefore, the real VSC1 active power output will be expressed by introducing a time constant τ in (12):

$$P_{VSC1}(p.u.) = P_{ref}(p.u.) \cdot \frac{1}{1+s\tau} \tag{12}$$

Accordingly, the total extra active power P_{IE} which supports the emulated inertial response consists of: 1) the portion provided by the dc link capacitors; and 2) the portion provided by the remote side grid through VSC1. P_{IE} will be released into the ac grid from the VSC3 where VQ control is adopted, which is expressed in (13):

$$P_{IE} = \Delta P_{VSC3,tot} = \Delta P_{VSC1} + P_{VSC3} \tag{13}$$

According to the swing equation for a SG, the ideal inertial response transfer function is illustrated in the lower blue box of Fig. 3. In comparison, the VSC IE control transfer function flow diagram is illustrated in the upper box of Fig. 3 which is derived based on (8)-(13).

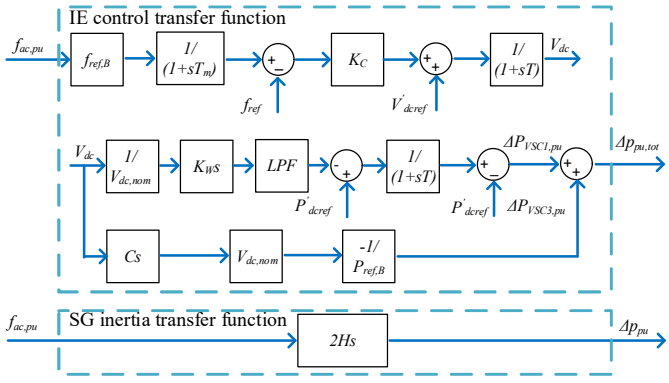

Fig. 3. The IE, SG *f-P* transfer function.

A Bode plot is used to observe the frequency response of the aforementioned transfer functions in order to evaluate the IE performance. The parameters illustrated in Fig. 3 are listed in Table I.

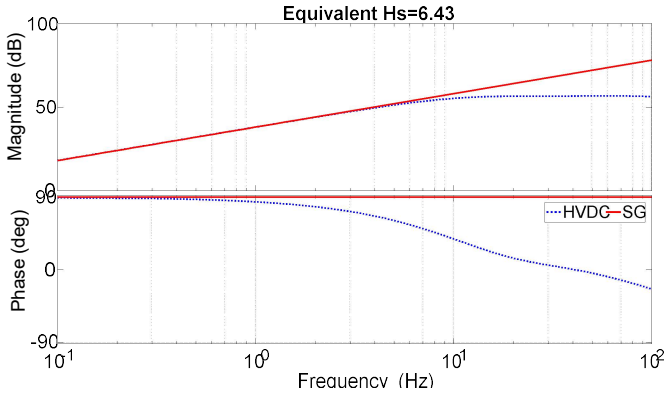

Fig. 4. Frequency response comparison between IE control and SG inertial response.

The IE control parameters are tuned to H_S =6.43s, which is close to the value of the typical turbine generators inertia constant. The frequency response of the transfer function is illustrated by the blue dashed curve in Fig. 4. In order to compare with the SG inertial response, the frequency response curve of the SG with the same inertia constant is also illustrated in Fig. 4 by the red curve. It can be observed that the two frequency response curves are very close to each other between the frequency range of 0.1Hz~1Hz, which is the performance bandwidth of the SG inertial response.

TABLE I. MTDC INERTIA EMULATION CONTROL PARAMETERS

$f_{ref,B}$	60 Hz	V_{dc0}	200 V
$P_{ref,B}$	2.5 kW	f_0	60 Hz
T_m	27 ms	C	5.4 mF
T	50 ms	S_{VSC}	2.5 kVA
K_C	77.16	M	1
K_W	0.21	N	4
LPF, ω_C	30 Hz		

B. PLL and Low Pass Filter Specification

The VSC phase-locked loop (PLL) and low pass filter, which are practically included in the VSC control modules, are also taken into consideration in the transfer function. The typical linearized PLL model is illustrated in Fig. 5 [23], where the phase detector (PD) is equivalent to the magnitude of the phase voltage V_m according to (14), and the PI controller is employed as the loop filter (LF). The PLL is equivalent to the first order transfer function if appropriately tuned. The time constant of the PLL is defined as T_m, which is expressed in the control block diagram in Fig. 3.

$$\widetilde{v_q} = V_m \sin(\theta_1 - \theta_2) \leftrightarrow PD = \frac{\widetilde{v_q}}{\tilde{\theta}} = V_m \tag{14}$$

The low pass filter block is placed after the K_WS block to filter out the high frequency harmonic components generated by the V_{dc} differentiation, and it can also be regarded as a first order transfer function expressed in (15).

$$LPF = \frac{\omega_C}{s+\omega_C} \tag{15}$$

It can be observed that the IE performance bandwidth will be influenced with the introduction of these practical modules, reflected as the magnitude and phase damping of the IE frequency response curve in Fig. 4. This will lead to a performance time delay compared with the real inertial response. The delay will be more and more significant with the increasing of the control module time delay. The IE effectiveness and accuracy will be negatively impacted if the frequency response of IE transfer function cannot track that of the SG inertia response within the concerned bandwidth.

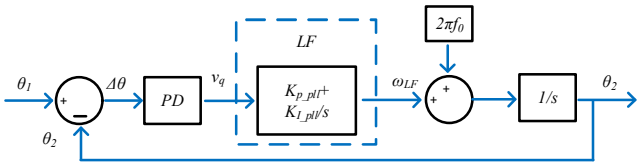

Fig. 5. Typical linearized PLL transfer function.

IV. Simulation Results

According to the analysis in Section III, there is a response delay introduced by the VSC control modules compared with the SG inertial response. Simulation tests were carried out to verify this phenomenon and evaluate its impact on the ac system. The 11-bus NPCC system model is selected as the main ac grid [22], which is shown in Fig. 5, where the generation units and loads in the ac system are denoted as G1~G5 and L7, L9, L12 and L13 respectively. Two cases with different system configurations are applied and compared. In Case 1, the MTDC network is adopted at bus 12 and bus 13, which is illustrated in the lower blue box in Fig. 6. In this case the remote SGs are connected to the main ac grid through the MTDC network. The inertia emulation control illustrated in Fig. 2 is employed in this case with an equivalent inertia constant H_S=6.43s, so all the extra active power providing the inertial support is released from the VSC3 at Bus 12 according to the design of the IE control. Case 2 is the control test, where the HVDC connection of the SG1 is replaced by a directly connected transmission line while the HVDC connection at bus 13 remains, which is illustrated in the upper blue box in Fig. 6. The inertia constant of the SG1 rotating mass is the same as H_S. A comparison between the SG inertial response and emulated inertial response can be observed by running the above two simulation cases respectively. The inertia constant of the 5 generation units G1~G5 are all defined as H_G=3s in order to reflect the low inertia future network with the high penetration of the renewable energy sources [24].

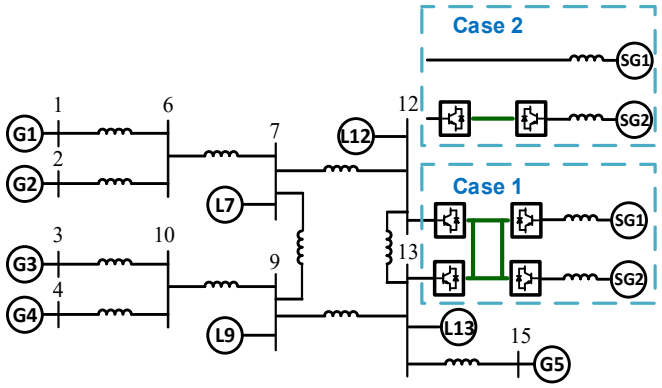

Fig. 6. Wind farm integrated NPCC system with HVDC transmission.

A. Load Increase at L7

A load increase scenario at L7 is analyzed in Matlab/ Simulink. The initial load condition of the generation units and the load of the local ac network is listed in Table II.

The L7 increases from P = 0.7 *p.u.* and Q = -0.1*p.u.* to P =1.4 *p.u.* and Q = -0.2 *p.u.* at t=71s. This load increase will immediately induce an ac system frequency drop according to the power system operating principle.

The active power injection curve at Bus 12 provided by the VSC3 in Case 1 and the directly connected SG1 in Case 2 is illustrated in Fig. 7(a). The SG active power injection P_{SG} is indicated by the solid black curve, which results from the inertial response of the generator rotating mass. According to Fig. 7(a), the P_{SG} increased sharply at the moment of load change, and gradually decrease to the previous value when the ac system frequency is stabilized.

The VSC3 active power injection P_{VSC3} is indicated by the red dashed curve. It can be observed that the power curves of P_{SG} and P_{VSC3} are very close to each other, except that the response of the VSC3 IE control lagged the SG inertial response by ~0.1s. This power injection delay verifies the analysis about the control response delay in Section III. Compared with the case adopting HVDC IE control, the VSC3 active power injection without IE control is illustrated by the pink dashed curve, where the P_{VSC3} is almost constant, indicating that no active power support is provided during the change of ac system frequency.

In order to have an overall evaluation of the main ac grid, G1~G5 are simulated in terms of the following indices: (1) Frequency nadir f_{nadir}; (2) RoCoF; (3) Phase angle $\Delta\theta$ difference between different buses directly connected by the generators. The results are illustrated in Fig. 8.

It can be observed from the figures in the first row of Fig. 8 that the output frequency curves of G1~G5 for Case 1 are similar to that for Case 2, indicating that the HVDC IE control provides a good inertial response. The frequency nadir zoom-in figures are illustrated in the second row of Fig. 8, where the frequency curve with IE control has a lower nadir point than that with a SG inertial response. Similarly, the RoCoF with IE control is greater than that with a real SG inertial response, especially right after the disturbance. The phase angle differences between the SG

connected buses are illustrated in the last row in Fig. 8, where a very slight increase of phase angle is observed.

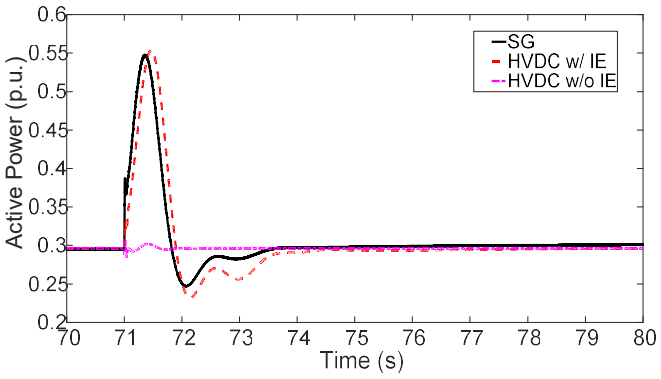

(a) Load increase scenario at Bus 7.

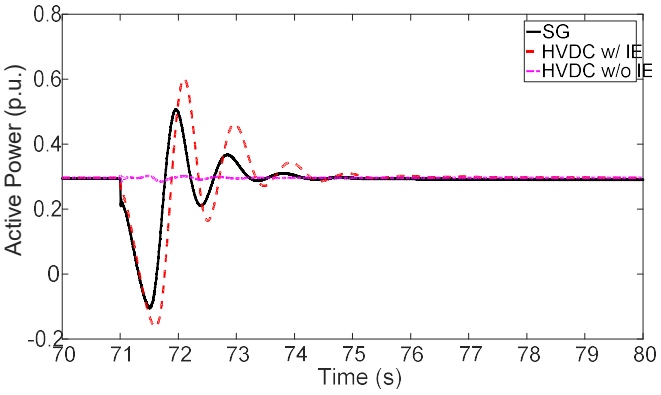

(b) Load decrease scenario at Bus 7.

Fig. 7. Active power output at Bus 12 after a disturbance, comparing the SG natural inertia response with the IE response provided by the HVDC converter.

TABLE II. AC SYSTEM INITIAL OPERATING CONDITION

Component	*P (p.u.)*	*Q (p.u.)*
L7	0.7	-0.1
L9	0.7	-0.1
L12	0.65	-0.1
L13	0.6	-0.1
VSC1	-0.3	0
VSC2	-0.3	0
VSC3	-0.3	0
VSC4	-0.3	0

B. Load Decrease at L7

load decrease scenario at L7 is analyzed in Matlab/ Simulink. The L7 decreases from $P = 0.7$ *p.u.* and $Q = -0.1$*p.u.* to $P = 0$ *p.u.* and $Q = 0$ *p.u.* at t=71s. In contrast with the load increase scenario, the load decrease will immediately induce an ac system frequency increase. The active power injection of the directly connected SG1 and the VSC3 at Bus 12 is illustrated in Fig. 7(b).

It can be observed that the P_{SG} dropped sharply at the moment of load change, and gradually increased back to the previous value when the ac system frequency went back to stabilization, which is indicated by the solid black curve. The VSC3 active power injection P_{VSC3} is indicated by the red dashed curve, and the active power contributed by VSC3 without IE control is illustrated by the pink dashed curve. The active power contribution curves of the SG1 and VSC3 have the same trend. Similar to the results in the load increase scenario, the response of the VSC3 IE control lags the SG1 inertial response by ~0.1s. The f_{nadir}, RoCoF, and phase angle $\Delta\theta$ are also evaluated in this scenario. The results are illustrated in Fig. 9. Similar to the results illustrated in Fig. 8, we can find that the output frequency, the RoCoF, and the phase angle difference between each generation units measured from the two cases respectively are overall close with each other. The results measured from Case 1 is slightly greater than the results from Case 2

It can be observed that the frequency response of the ac system with the MTDC inertia emulation control is very close to that with an equivalent SG according to Fig. 8 and Fig. 9. However, the inertia emulation control cannot instantaneously respond to the system power imbalance, resulting in a delayed active power contribution. So the frequency nadir and the RoCoF of each generation unit in Case 1 are greater than those in Case 2 in both test scenarios. However, by observing the active power contribution in Fig. 7 and the system frequency curve in Fig. 8 and Fig. 9, we found that both two cases follow the same trend of frequency response. The MTDC inertia emulation control can achieve a similar inertial response compared with that of the SG. The control response delay will lead to an active power injection delay, so a greater f_{Nadir}, RoCoF and phase angle difference is observed.

V. CONCLUSION

The MTDC network impact on the IE performance is analyzed in this paper. The analysis indicates that the HVDC IE performance can be nearly as good as the inertial support provided by the directly connected ac subsystem with a relatively high inertia constant. The response delay introduced by the VSC station control modules will correspondingly introduce a delay to the IE performance, which will further the frequency nadir f_{Nadir} and RoCoF. Furthermore, the effectiveness of the inertia emulation will be compromised if the delay time is too long. Therefore, the inertia emulation control is required to be carefully designed in order to achieve a good inertial response.

ACKNOWLEDGMENT

This work is supported by the Center for Ultra-Wide-Area Resilient Electric Energy Transmission Networks (CURENT).

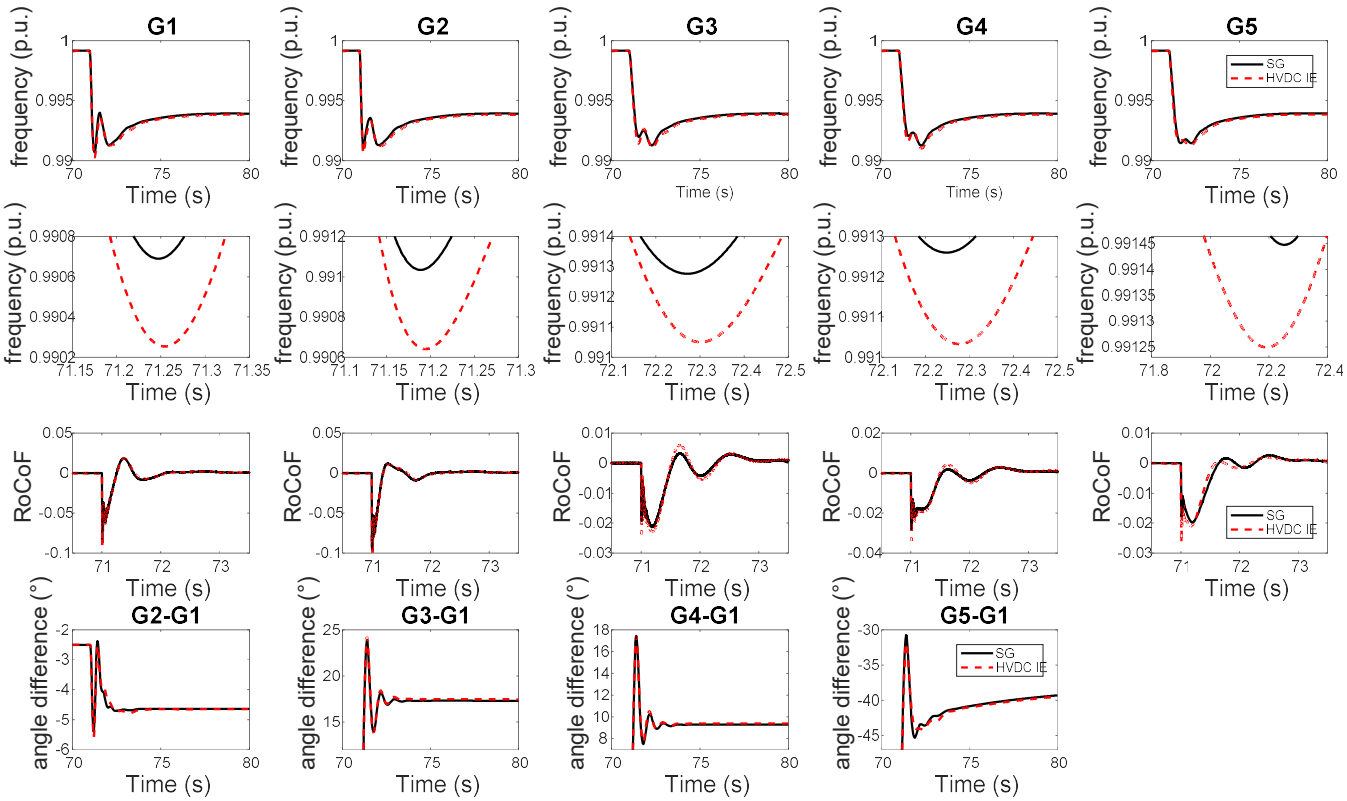

Fig. 8. G1- G5 f_{nadir}, RoCoF and G2-G1, G3-G1, G4-G1, G5-G1 phase angle difference for step load increase scenario.

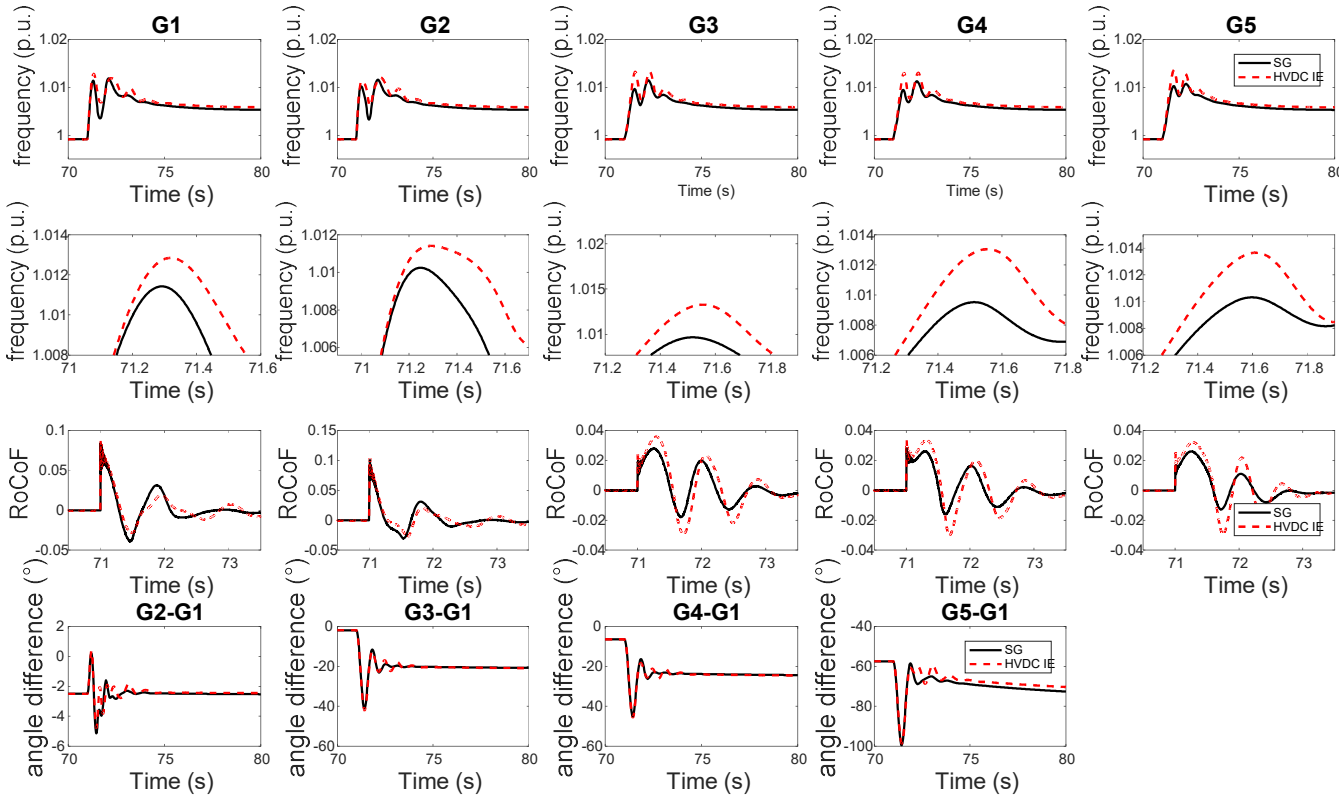

Fig. 9. G1- G5 f_{nadir}, RoCoF and G2-G1, G3-G1, G4-G1, G5-G1 phase angle difference for step load decrease scenario.

REFERENCES

[1] P. Bresesti, W. L. Kling, R. L. Hendriks, and R. Vailati, "HVDC connection of offshore wind farms to the transmission system, " in *IEEE Trans. Energy Convers*, vol. 22, no. 1, pp. 37–43, Mar. 2007.

[2] J. Liang, T. Jing, O. Gomis-Bellmunt, J. Ekanayake and N. Jenkins, "Operation and control of multiterminal HVDC transmission for offshore wind farms," in *IEEE Trans. on Power Delivery*, vol. 26, no. 4, pp. 2596-2604, Oct. 2011.

[3] J. Zhu, C. D. Booth, G. P. Adam, A. J. Roscoe and C. G. Bright, "Inertia emulation control strategy for VSC-HVDC transmission systems," in *IEEE Trans. Power Systems*, vol. 28, no. 2, pp. 1277-1287, May 2013.

[4] B. Silva, C. L. Moreira, L. Seca, Y. Phulpin and J. A. Pecas Lopes, "Provision of inertial and primary frequency control services using Offshore multiterminal HVDC networks," in *IEEE Trans. Sustainable Energy*, vol. 3, no. 4, pp. 800-808, Oct. 2012.

[5] O. D. Adeuyi et al., "Frequency support from modular multilevel converter based multi-terminal HVDC schemes," in *Proc. IEEE Power & Energy Society General Meeting*, Denver, CO, 2015, pp. 1-5.

[6] M. Suwan and I. Erlich, "Frequency control by HVDC connected offshore wind farms for overfrequency limitation," in *Proc. IEEE International Energy Conference (ENERGYCON)*, Leuven, 2016, pp. 1-6.

[7] M. Suwan and I. Erlich, "Overfrequency limiting control by VSC-HVDC connected offshore WFs," in *Proc. IEEE Power & Energy Society General Meeting*, Denver, CO, 2015, pp. 1-5.

[8] M. Yu, A. Dyśko, C. D. Booth, A. J. Roscoe and J. Zhu, "A review of control methods for providing frequency response in VSC-HVDC transmission systems," in *International Universities Power Engineering Conference (UPEC)*, Cluj-Napoca, 2014, pp. 1-6.

[9] H. Liu and Z. Chen, "Contribution of VSC-HVDC to frequency regulation of power systems with offshore wind generation," in *IEEE Trans on Energy Conversion*, vol. 30, no. 3, pp. 918-926, Sept. 2015.

[10] M. Benidris, S. Elsaiah, S. Sulaeman and J. Mitra, "Transient stability of distributed generators in the presence of energy storage devices," in *North American Power Symposium (NAPS)*, Champaign, IL, 2012, pp. 1-6.

[11] G. Delille, B. Francois and G. Malarange, "Dynamic frequency control support by energy storage to reduce the impact of wind and solar generation on isolated power system's inertia," in *IEEE Trans on Sustainable Energy*, vol. 3, no. 4, pp. 931-939, Oct. 2012.

[12] S. Alepuz, A. Calle, S. Busquets-Monge, S. Kouro and B. Wu, "Use of stored energy in PMSG rotor inertia for Low-Voltage Ride-Through in Back-to-Back NPC converter-based wind power systems," in *IEEE Trans on Industrial Electronics*, vol. 60, no. 5, pp. 1787-1796, May 2013.

[13] Ji-eun Yi et al., "Micro flywheel energy storage system with axial flux machine," in *IEEE/ASME international conference on advanced intelligent mechatronics*, Zurich, 2007, pp. 1-6.

[14] X. Feng, "Dynamic balancing for low inertia power systems," in *IEEE Power & Energy Society General Meeting*, Vancouver, BC, 2013, pp. 1-5.

[15] V. Trovato, S. H. Tindemans and G. Strbac, "Demand response contribution to effective inertia for system security in the GB 2020 gone green scenario," in *IEEE PES ISGT Europe*, Lyngby, 2013, pp. 1-5.

[16] J. Zhu, J. M. Guerrero, C. D. Booth, H. Zhang and G. P. Adam, "A generic inertia emulation controller for multi-terminal VSC-HVDC systems," *in Proc. 2nd IET Renewable Power Generation Conference*, Beijing, 2013, pp. 1-6.

[17] J. Zhu, J. M. Guerrero, W. Hung, C. D. Booth and G. P. Adam, "Generic inertia emulation controller for multi-terminal voltage-source-converter high voltage direct current systems," in *IET Renewable Power Generation,* vol. 8, no. 7, pp. 740-748, September 2014.

[18] Y. Pipelzadeh, B. Chaudhuri and T. C. Green, "Inertial response from remote offshore wind farms connected through VSC-HVDC links: A Communication-less scheme," in *IEEE Power and Energy Society General Meeting*, San Diego, CA, 2012, pp. 1-6.

[19] Y. Phulpin, "Communication-free inertia and frequency control for wind generators connected by an HVDC-Link," in *IEEE Trans on Power Systems*, vol. 27, no. 2, pp. 1136-1137, May 2012.

[20] Y. Li, Z. Zhang, Y. Yang, Y. Li, H. Chen, Z. Xu, "Coordinated control of wind farm and VSC–HVDC system using capacitor energy and kinetic energy to improve inertia level of power systems, " in *International Journal of Electrical Power & Energy Systems*, Volume 59, Pages 79-92, 2014.

[21] X. Liu and A. Lindemann, "Coordinated control of VSC-HVDC connected offshore windfarms for enhanced ability of providing synthetic inertia," in *International Symposium on Power Electronics for Distributed Generation Systems (PEDG)*, Aachen, 2015, pp. 1-6.

[22] S. Zhang, Y. Li and F. Wang, "Impact of DC fault in multi-terminal DC grid on connected AC system stability," *IEEE Energy Conversion Congress and Exposition (ECCE)*, Cincinnati, OH, 2017, pp. 2651-2658.

[23] D. Dong, J. Li, D. Boroyevich, P. Mattavelli, I. Cvetkovic and Y. Xue, "Frequency behavior and its stability of grid-interface converter in distributed generation systems," in *IEEE Applied Power Electronics Conference and Exposition (APEC)*, Orlando, FL, 2012, pp. 1887-1893.

[24] C. Yuan, M. Illindala, A. Khalsa, “Co-Optimization scheme for energy resource planning in community microgrids,” in *IEEE Transactions on Sustainable Energy*, vol. 8, no. 4, pp. 1351-1360, Oct. 2017.